SCHOOL OF COMPUTATION, INFORMATION AND TECHNOLOGY — INFORMATICS

TECHNISCHE UNIVERSITÄT MÜNCHEN

Master's Thesis in Informatics

Design and Control of an Aerodynamic Surface-Enhanced Multirotor

William Constantin Rosenhahn

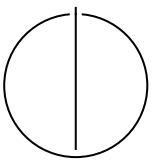

SCHOOL OF COMPUTATION, INFORMATION AND TECHNOLOGY — INFORMATICS

TECHNISCHE UNIVERSITÄT MÜNCHEN

Master's Thesis in Informatics

Design and Control of an Aerodynamic Surface-Enhanced Multirotor

Author:	William Constantin Rosenhahn
Examiner:	Prof. Dr.-Ing. Markus Ryll
Supervisor:	Lukas Pries
Submission Date:	01.12.2025

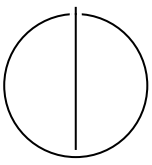

I confirm that this master's thesis is my own work and I have documented all sources and material used.

Munich, 01.12.2025 William Constantin Rosenhahn

Acknowledgments

Abstract

Contents

1 Introduction

1.1 Motivation

Micro air vehicles (MAVs) with efficient autonomous navigation can strengthen applications such as search-and-rescue and last-mile delivery, where safety, robustness, and endurance are critical. Conventional quadrotors offer agility and precise control but are power-inefficient in sustained forward flight. Fixed-wing platforms are efficient but cannot hover and are less maneuverable in confined spaces. Hybrid vertical take-off and landing (VTOL) concepts improve mission versatility but increase mechanical and control complexity. This thesis investigates an intermediate design: a multirotor augmented with fixed aerodynamic surfaces to harvest passive lift during horizontal motion while keeping multirotor agility.

1.2 Problem statement and scope

In the presence of aerodynamic surfaces, hard-to-model aerodynamic forces become significant and challenge controller design. We aim to develop a platform and control strategy that:

- preserves quadrotor agility while improving forward-flight efficiency via passive lift,
- tracks agile trajectories accurately without requiring aerodynamic parameter identification, and
- remains robust to modeling errors and disturbances.

The central question is whether an Incremental Nonlinear Dynamic Inversion (INDI)-based controller can achieve accurate trajectory tracking on an aerodynamic surface-enhanced quadrotor without an explicit aerodynamic model.

1.3 Contributions

This thesis presents:

- a design of an aerodynamic surface-enhanced quadrotor in X-wing configuration,
- a dynamics model combining a standard quadrotor 6-DoF model with simplified quadratic lift/drag,
- a trajectory-tracking controller based on geometric control and INDI, including a coordinated-turn option, and
- an experimental evaluation: thrust-map identification, agility/controllability, aerodynamic disturbance characterization, and efficiency assessment.

1.4 Thesis organization

Chapter 3 reviews related work and motivates the chosen design. Chapter 4 details the platform. Chapter 5 derives the model. Chapter 6 presents the controller. Chapters **??** and 7 describe the setup and experiments. Chapter 8 concludes.

2 Background

This chapter introduces foundational concepts relevant to agile and efficient autonomous flight with aerodynamic surface-enhanced multirotors. It briefly covers flight vehicle classes, 6-DoF rigid-body kinematics and dynamics, and aerodynamic fundamentals (lift, drag, moments) used later in the modeling and control chapters.

2.1 Aerial vehicle classes

We distinguish multirotors, fixed-wing aircraft, tailsitters, and general VTOL hybrids. Key trade-offs include agility, efficiency, range, and controllability. Hybrids aim to combine vertical take-off and landing with efficient forward flight.

2.2 Rigid-body frames and notation

We use an inertial/world frame $\{\mathcal{I}\}$ and a body frame $\{\mathcal{B}\}$. Position $\mathbf{p} \in \mathbb{R}^3$, velocity $\mathbf{v}$, orientation $R \in SO(3)$, angular velocity $\boldsymbol{\omega} \in \mathbb{R}^3$. Standard hat/vee maps and skew operator $[\cdot]_\times$ are adopted.

2.3 Aerodynamic preliminaries

Lift $L = \frac{1}{2}\rho V^2 S C_L(\alpha)$ and drag $D = \frac{1}{2}\rho V^2 S C_D(\alpha)$, with α the angle of attack, reference area S, and air density ρ. For small angles or thin-airfoil approximations, $C_L \approx a_\alpha \alpha$, $C_D \approx C_{D0} + k C_L^2$. These models motivate the simplified quadratic lift/drag used in Chapter 5.

3 Related Work

Designing a UAV that is both agile (e.g., sustained $\geq 3\,g$ banked turns on meter-scale radii with low tracking error) and energy-efficient (low Wh/km or J/m at cruise), while remaining controllable across hover and forward flight, robust to aerodynamic disturbances, and implementable with moderate complexity, requires weighing trade-offs across canonical configurations: multirotors, fixed-wing, tailsitters, tiltrotors/tilt-wings, and quadplane VTOLs. We additionally review "aerodynamically augmented" multicopters—i.e., quadrotors with small fixed lifting surfaces or shrouds—because they can mitigate the multirotor's forward-flight inefficiency without incurring the full complexity of morphing hybrids.

3.1 Baselines: Agility vs. Efficiency

Pure multirotors Pure multirotors excel in agility and controllability in hover and low-speed flight. State-of-the-art quadrotors routinely track aggressive trajectories at 2–5 g and 40–70 km/h with centimeter-level RMS errors using differential-flatness feedforward plus robust inner loops—often incremental nonlinear dynamic inversion (INDI) [**Tal2018**; **Tal2021**; **Foehn2022**]. For example, Tal and Karaman report tracking at 12.9 m/s with up to 2.1 g and 6.6 cm RMS error, and explicit robustness to added drag and rope pulls due to INDI's disturbance-rejection properties [**Tal2018**]. Foehn et al.'s Agilicious platform demonstrates up to $\sim$5 g and $\sim$70 km/h autonomous tracking with modern model-predictive and differential-flatness-based controllers, again emphasizing agility and controllability [**Foehn2022**]. However, multirotors are energetically inefficient in forward flight because thrust must be tilted to produce lift and drag grows quickly with speed.

Fixed-wing aircraft By contrast, fixed-wing aircraft achieve much lower J/m at cruise because wings supply lift with high L/D, but they cannot hover.

Hybrids: tailsitters, tiltrotors, and quadplanes Tailsitters and tiltrotor/tilt-wing hybrids attempt to combine both: hover on rotors, then transition to wing-borne flight for efficiency. Recent tailsitter work shows promising agility and envelope coverage—e.g.,

Lu et al. report 10–20 m/s trajectories with ∼2.5 g agile maneuvers using a flatness-based planner and robust tracking [**Lu2022**], and Tal and Karaman demonstrate global trajectory-tracking and agile uncoordinated flight (e.g., sideways/knife-edge) using a global INDI framework [**Tal2021Tailsitter**; **Tal2022Global**]. Tilt-wing/tilt-rotor concepts have matured in modeling and flight-dynamics/transitions (e.g., Daud Filho et al. present dynamic models and simulated transition trajectories for a canard-plus-wing tilt concept) but remain mechanically and algorithmically complex, with challenging cross-couplings during transitions [**DaudFilho2024**; **Misra2022**]. Quadplanes (fixed wing + vertical-lift rotors) offer practical VTOL with cruise efficiency; experimental examples (e.g., a tandem-wing quadplane) target long-range VTOL with simpler mechanisms than tilting actuators, though added mass/drag can degrade hover agility and gust robustness [**Okulski2022**].

3.2 Controller Classes Used Across the Spectrum

Geometric SE(3) control established a rigorous foundation for aggressive multirotor tracking with global attitude representations [**Lee2010**] and geometric adaptive variants handle parametric uncertainties [**Goodarzi2015**]. Differential-flatness-based planning/-control (e.g., minimum-snap) is ubiquitous for trajectory generation and feedforward tracking [**Mellinger2011**; **Tal2018**]. INDI has become a go-to inner-loop choice for robustness to unmodeled aero forces/torques at high speed and in gusts [**Sieberling2010**; **Smeur2017**]. A direct empirical comparison on agile quadrotor flight found that both NMPC and differential-flatness-based controllers benefit markedly (≈78% error reduction) from coupling to an INDI inner loop and drag modeling at speeds up to 20 m/s [**Sun2021**]. These results are important because the proposed quad-with-small-wings concept aims to keep a multirotor control stack (differential-flatness/geometric + INDI) while adding lightweight aerodynamics.

3.3 Aerodynamic Augmentation on Multicopters

The most directly relevant evidence comes from micro-to-small UAVs that add fixed lifting surfaces to multirotors:

Small wings Dawkins and DeVries integrated small wings on a micro-quad and quantified the trade-off: ∼35% energy saving in forward flight, but ∼45% extra power in hover due to added mass/drag; the wing "pays off" beyond ∼3–5 m/s depending on angle-of-attack and prop wash interaction [**Dawkins2018**]. They report smoother

tracking and reduced pitch angles at speed, indicating improved controllability in forward flight, but some hover agility penalty.

Xiao et al. designed a "lifting-wing fixed on multirotor" with a decoupled wing mount. On a 1.2 kg quad, they measured 50.14% less electrical power at 15 m/s compared with the bare quad; optimal cruise power shifted from ≈200–250 W down to ≈100–125 W with the wing, without major changes to the multirotor controller [**Xiao2020**]. This is a strong, quantitative demonstration that small fixed aerodynamic surfaces can more than halve J/m at moderate forward speeds while preserving conventional quad control.

Airfoilized arms Freitas et al. systematically tested airfoilized arms on a quad (DJI F450 class). Arm airfoils reduced arm drag and delivered ∼19–31% less electrical power in forward flight at 10–15 m/s (depending on angle) and modest improvements to top speed, with negligible hover penalty and no controller change [**Freitas2025**]. This is especially attractive for "agility-first" designs where we seek free forward-flight efficiency.

Summary These works collectively show that adding small lifting/streamlining surfaces to a quad yields measured cruise efficiency gains (≈20–50% power reduction at ≈10–15 m/s) at minimal implementation cost: no tilting mechanisms, no transitions, and only modest or negligible changes to hover agility if the surfaces are small and decoupled from rotor flows. Importantly, the canonical quadrotor controller stack (geometric/differential-flatness + INDI inner loop) remains applicable, maintaining excellent tracking (∼few-cm RMS) and high gust robustness documented for agile quads [**Tal2018**; **Foehn2022**; **Sun2021**].

3.4 Shrouds and Ducts as Augmentation

Shrouding improves hover power loading and can protect the rotors. MDPI Drones studies report ∼15–28% improvements in lift and "FM efficiency" for optimized ducted multi-propeller configurations in hover [**Li2021**]. Classic MAV shroud experiments show up to ∼30% power-loading gains at small scales [**Hrishikeshavan2014**], and broader surveys note up to >50% thrust gains or equivalent power reductions in hover for well-designed ducts, but performance degrades at higher advance ratios (forward flight) due to inlet losses and added frontal area [**Chew2021**; **Pereira2008**]. Thus, shrouds are advantageous for hover/low-speed efficiency and safety but can hurt high-speed efficiency and cross-wind agility—less aligned with our "agile forward-flight efficiency" goal.

3.5 Quantitative Comparison Across Criteria

From the studies above:

Agility Pure multirotors: $\geq 3\,g$, $\leq 0.1\,\mathrm{m}$ RMS tracking demonstrated [**Tal2018**; **Foehn2022**]. Tailsitters: agile aerobatics and 2–3 g transitions are feasible [**Lu2022**; **Tal2022Global**], but hover control surfaces may be saturation-limited in gusts. Quadplanes/tilt designs: agility is generally lower in hover due to added inertia and interference; transitions add constraints [**Okulski2022**; **Misra2022**].

Efficiency (forward flight) Small fixed wings/airfoils on quads reduce cruise power by ∼20–50% at 10–15 m/s [**Dawkins2018**; **Xiao2020**; **Freitas2025**]. Shrouds: +15–30% hover power loading, but often worse at higher advance ratios [**Li2021**; **Hrishikeshavan2014**; **Chew2021**]. Hybrids (tilt/quadplane/tailsitter) achieve fixed-wing-like J/m at cruise but pay complexity/weight penalties.

Controllability & transitions Multirotors and "quad + small wings" avoid mode transitions entirely—hover/forward authority comes from the same actuators; differential-flatness/geometric + INDI covers both regimes [**Lee2010**; **Tal2018**]. Hybrids require transition path planning and mode-dependent control allocation [**DaudFilho2024**; **Misra2022**].

Robustness to aero disturbances INDI-based quads show strong disturbance rejection without precise aero models [**Sieberling2010**; **Smeur2017**; **Sun2021**]. Hybrids can be robust, but robustness proofs and quantitative gust testing during transition remain sparse.

Implementation complexity Adding small fixed surfaces is mechanically trivial and controller-agnostic; shrouds add structure and possible crosswind penalties; hybrids add mechanisms, sensors, and software complexity (e.g., NMPC with switching and detailed aerodynamics).

3.6 Gaps and Open Issues

Despite progress, three gaps remain:

1. There are few quantitative studies of small, fixed wings on quads that explicitly preserve aggressive maneuverability ($\geq 3\,g$, meter-scale turns) while reporting

cruise Wh/km (or J/m) and closed-loop tracking error; most report % power savings at one speed [**Dawkins2018**; **Xiao2020**].

2. Disturbance modeling for augmented quads is incomplete, particularly interactions between rotor wakes and small wings across the speed envelope and in crosswinds; robust INDI masks some deficiencies, but better disturbance observers/models would inform design trade-offs [**Sun2021**].

3. For hybrid VTOLs, coordinated-turn performance (load factors, radius, sideslip limits) with full transition dynamics is under-reported; Daud Filho et al. detail transitions but not coordinated turns with quantitative lateral-acceleration margins [**DaudFilho2024**].

These gaps motivate a design that seeks measured efficiency gains with minimal impact on agility and low complexity.

3.7 Why a Quadrotor with Small Fixed Aerodynamic Surfaces?

The literature supports a clear argument:

1. **Preserve hover agility and controllability**: no transitions, mature differential-flatness/geometric + INDI stack with proven centimeter-level tracking and multi-g maneuvers [**Lee2010**; **Tal2018**; **Foehn2022**].

2. **Capture meaningful cruise-efficiency gains**: $\sim$20–50% power reduction around 10–15 m/s using small wings or airfoilized arms [**Dawkins2018**; **Xiao2020**; **Freitas2025**], directly lowering J/m and extending range/mission time without complex mechanisms.

3. **Maintain robustness to disturbances via INDI** without high-fidelity aero models [**Sieberling2010**; **Smeur2017**; **Sun2021**].

4. **Keep implementation complexity low**: fixed surfaces; unchanged propulsion and control allocation, avoiding the mass, moving parts, and software overhead of tilt/transition systems [**Misra2022**; **Okulski2022**].

Given the target criteria—agility, efficiency at cruise, controllability across the envelope, gust robustness, and modest complexity—the evidence favors a quadrotor with small fixed aerodynamic surfaces over more complex hybrids.

4 Platform Design

We design an aerodynamic surface-enhanced quadrotor in X-wing configuration to preserve multirotor agility while benefiting from passive lift in forward flight.

4.1 Configuration and layout

- Quadrotor X configuration with integrated fixed wings (X-shaped planform) aligned with the rotor arms. - Structural considerations: wing aspect ratio, sweep/dihedral, stiffness, and mounting relative to CoG and rotor thrust lines. - Sensors and avionics: IMU, FC/ESCs, Jetson companion, motion capture (Vicon) for ground-truth.

4.2 Wing and aerodynamic surface choices

- Select planform and airfoil balancing lift at operational Reynolds numbers with low added mass. - Wing area and placement trade-offs: lift vs. added drag and control cross-coupling; ensure propeller inflow interactions are manageable.

4.3 Propulsion and actuation

- Motor-propeller pair sized for required thrust-to-weight and agility margins (e.g., 3g lateral load tracking). - Thrust and torque maps: throttle-to-RPM and RPM-to-thrust/torque characterization to support control allocation.

5 Dynamics Model

We derive a 6-DoF rigid-body model of the platform with rotor thrust/torque and simplified aerodynamic forces/moments from the integrated wings.

5.1 Frames, states, and inputs

States: $(\mathbf{p}, \mathbf{v}, R, \boldsymbol{\omega}) \in \mathbb{R}^3 \times \mathbb{R}^3 \times SO(3) \times \mathbb{R}^3$. Inputs: rotor thrusts $\mathbf{u} = [f_1, \ldots, f_4]^\top$ (or RPM), combined into total thrust f_T and body torques $\boldsymbol{\tau}$ by allocation matrix G.

5.2 Forces and moments

- Gravity: $m\mathbf{g}$. - Rotor thrust in body z: $\mathbf{F}_T = -f_T\, R\mathbf{e}_3$ (world frame). - Aerodynamics (simplified): wing lift and drag quadratic in body-frame airspeed $\mathbf{v}_a = \mathbf{v} - \mathbf{v}_w$ transformed to the body.

$$L = \tfrac{1}{2}\rho S C_L(\alpha)\|\mathbf{v}_a\|^2, \qquad D = \tfrac{1}{2}\rho S C_D(\alpha)\|\mathbf{v}_a\|^2. \tag{5.1}$$

We use $C_L = a_\alpha \alpha$, $C_D = C_{D0} + kC_L^2$ or the compact quadratic form $\mathbf{F}_{\text{aero}} = -k_D \|\mathbf{v}_a\| \mathbf{v}_a + k_L \|\mathbf{v}_a\| \mathbf{v}_\perp$ with $\mathbf{v}_\perp$ orthogonal to the surface.

Moments from aerodynamic center offset and rotor torques are aggregated into $\boldsymbol{\tau} = G_\tau \mathbf{u} + \boldsymbol{\tau}_{\text{aero}}$.

5.3 Equations of motion

$$\dot{\mathbf{p}} = \mathbf{v}, \tag{5.2}$$
$$\dot{\mathbf{v}} = \tfrac{1}{m}\big(m\mathbf{g} + \mathbf{F}_T + R\,\mathbf{F}_{\text{aero}}\big), \tag{5.3}$$
$$\dot{R} = R\,[\boldsymbol{\omega}]_\times, \tag{5.4}$$
$$J\dot{\boldsymbol{\omega}} = -\boldsymbol{\omega} \times J\boldsymbol{\omega} + \boldsymbol{\tau}. \tag{5.5}$$

Assumptions: quasi-steady aerodynamics, negligible prop-wash coupling in first-order model, parameter lumping for identification.

6 Control Architecture

We design a trajectory-tracking controller combining geometric position/attitude control with Incremental Nonlinear Dynamic Inversion (INDI). Differential flatness provides reference generation. INDI reduces dependence on aerodynamic modeling and handles unmodeled disturbances.

6.1 Reference generation

Trajectory references $(\mathbf{p}_d, \dot{\mathbf{p}}_d, \ddot{\mathbf{p}}_d, \psi_d)$ from a flatness-based planner or minimum-snap polynomial, optionally enforcing coordinated-turn constraints in forward flight to bound sideslip.

6.2 Outer-loop (geometric SE(3))

Compute desired body z-axis from force command $\mathbf{f}_d = m(\ddot{\mathbf{p}}_d + \mathbf{k}_p\tilde{\mathbf{p}} + \mathbf{k}_v\tilde{\mathbf{v}} - \mathbf{g})$ and yaw ψ_d, yielding desired attitude R_d and thrust f_T.

6.3 Inner-loop INDI

Using measured specific force and angular rates, INDI updates actuator commands incrementally:

$$\Delta\mathbf{u} = G^{-1}\left(\mathbf{y}_d - \mathbf{y}\right), \tag{6.1}$$

where $\mathbf{y}$ are directly measurable accelerations/attitude-rate related outputs. The key insight is that unmodeled aerodynamics cancel in the increment under small sampling intervals, leaving a local input-output mapping identified online via control effectiveness. See [**Smeur2016**; **Oosedo2017**; **vanKampen2018**] and [**Tzoumanikas2021**] for agile INDI on aerial platforms.

6.3.1 Aerodynamic cancellation argument

Let $\dot{\mathbf{y}} = f(\cdot) + B\,\mathbf{u} + \mathbf{d}$ with disturbance/aerodynamics $\mathbf{d}$. Over short intervals Δt, the change satisfies $\Delta\mathbf{y} \approx B\,\Delta\mathbf{u}$ as $\Delta\mathbf{d}$ is second-order. Thus the incremental control law does not require explicit aerodynamic parameters.

6.4 Coordinated turn option

Impose sideslip $\beta \approx 0$ by aligning drag with body-x projected velocity and setting a yaw rate command consistent with lateral acceleration: $\dot{\psi} \approx a_y/(V\cos\theta)$ at moderate bank angles.

6.5 Experimental Setup

This section documents the hardware configuration, software stack, and test facilities that enabled the experimental evaluation of the aerodynamic surface-enhanced quadrotor. The setup was designed to be fully reproducible, with all control and estimation software running on open frameworks and all data recorded for subsequent analysis.

6.5.1 Hardware

Airframe and Propulsion

The experimental platform consists of an X-wing aerodynamic surface-enhanced quadrotor with a total mass of 2.5 (without batteries: 1.75). Each of the four T-MOTOR VELOX V2808 motors produces a maximum static thrust of approximately 22, resulting in a total available thrust of 88 and a thrust-to-weight ratio of 3.59 at nominal 22.2 (6S LiPo). The propulsion system employs HQProp 7×3.5×3 three-blade racing propellers optimized for medium–high efficiency in the forward-flight regime.

The wings feature a NACA 0015 airfoil with a span of 450 and a chord of 250. Four identical fixed wings are arranged orthogonally (90 between adjacent wings) and mounted with alternating dihedral and anhedral angles of ±45. The wings are attached to the central frame using two carbon spars (10 outer diameter) clamped into the core structure, allowing for fast removal. The center frame and motor mounts are 3D-printed from standard PLA, while the wing surfaces are printed from lightweight PLA Aero. The total projected horizontal area of all wings is approximately $S_t = 0.318$.

Each motor is mounted with a 5 outward tilt to improve yaw authority through differential thrust vectoring. The center of gravity is located at the geometric center of

the vehicle, aligned with the midpoint between all four motors, and approximately at one quarter of the wing chord length from the leading edge.

Avionics and Electrical System

The avionics stack is based on a *Kakute H7 v1.5* flight controller paired with a 4-in-1 ESC. Two 1400 6S Tattu R-Line batteries are connected in parallel to power the propulsion and avionics subsystems, resulting in an effective 2800 capacity. The onboard computer, an NVIDIA Jetson Orin Nano (8 GB, JetPack 6), is powered independently from a 1800 4S LiPo battery through a buck converter.

A custom-modified version of *Betaflight* firmware was employed on the flight controller to extract motor RPM and battery voltage data from the DShot interface and stream them over MAVLink. This modification was necessary because the stock Betaflight implementation does not support publishing these telemetry values via MAVLink. The onboard IMU integrated into the Kakute H7 was used for all experiments; no external IMUs were installed. Vicon markers were arranged asymmetrically to ensure unambiguous pose tracking.

Table 6.1: Bill of Materials (BOM) for the experimental platform.

Category	Component	Model / Key Specs
Airframe	Frame	X-wing center frame with carbon wing spars
Airframe	Wings	4× fixed wings (450×250 mm, NACA 0015, ±45° dihedral)
Propulsion	Motors (×4)	T-MOTOR VELOX V2808, max 22 N each
Propulsion	Propellers (×4)	HQProp 7×3.5×3, 3-blade
Avionics	FC + ESC	Kakute H7 v1.5 Stack (4-in-1 ESC)
Power	Battery (×2, parallel)	Tattu R-Line V5.0 6S 1400 mAh (150C), XT60
Companion	Computer	Jetson Orin Nano 8 GB, CUDA 12, Ubuntu 22.04
Companion	Power	Tattu R-Line V3.0 4S 1800 mAh (120C), buck regulated
Motion Capture	Markers	4× 2 cm asymmetric constellation

6.5.2 Software

Architecture and Communication

The onboard software stack consists of *ROS 1 Noetic* running on the Jetson companion. The geometric controller with inner and outer INDI (Incremental Nonlinear Dynamic Inversion) loops was implemented in ROS and executed on the companion, which sent individual motor speed commands directly to the flight controller over MAVLink via

UART. The flight controller, in turn, only relayed the received motor commands to the ESCs while providing IMU, motor RPM, and battery telemetry back to the companion.

A ROS master node was hosted on a ground station computer, while the Jetson ran a ROS node for flight control and data logging. Communication between the two systems was established via Wi-Fi. The ground station handled trajectory loading, arming, and manual control interfaces. All experiment data, including position, velocity, attitude, thrust commands, and battery voltage, were logged in *rosbag* format for offline analysis in Python.

Estimation and Control

The state estimation pipeline used the Vicon motion capture system to provide real-time position and attitude feedback to the controller. In some experiments, an onboard Extended Kalman Filter (EKF) fused IMU data for state estimation. The Vicon system and onboard IMU operated in a consistent right-handed coordinate convention (front–left–up), with roll about the x-axis, pitch about y, and yaw about z.

All flight maneuvers, including point-to-point transitions and trajectory tracking, were executed fully autonomously from predefined setpoints. No separate failsafe was implemented for Vicon loss, but trajectories could be manually stopped and the vehicle landed or disarmed from the base station.

6.5.3 Facilities

Motion Capture Systems

Two different Vicon systems were employed for data acquisition and feedback. The smaller test arena in Munich measured approximately 7×8 and was used primarily for agility experiments, such as 3g circle maneuvers. The larger *AIDA Hall* at Reutlingen University provided a volume of about 60×45, enabling steady forward-flight efficiency trials (see Fig. 6.1). Both systems operated at a sampling rate of 200. Vicon data were used both as ground truth and as feedback for the control loop.

Test Protocols

Agility tests were performed in the Munich indoor arena equipped with safety nets and a soft landing surface. Efficiency tests were conducted in the AIDA Hall under still-air indoor conditions, with no wind sources or obstacles. Energy consumption was estimated from measured voltage, current draw, and propeller rotational speed data. Typical flight durations were approximately five minutes per run.

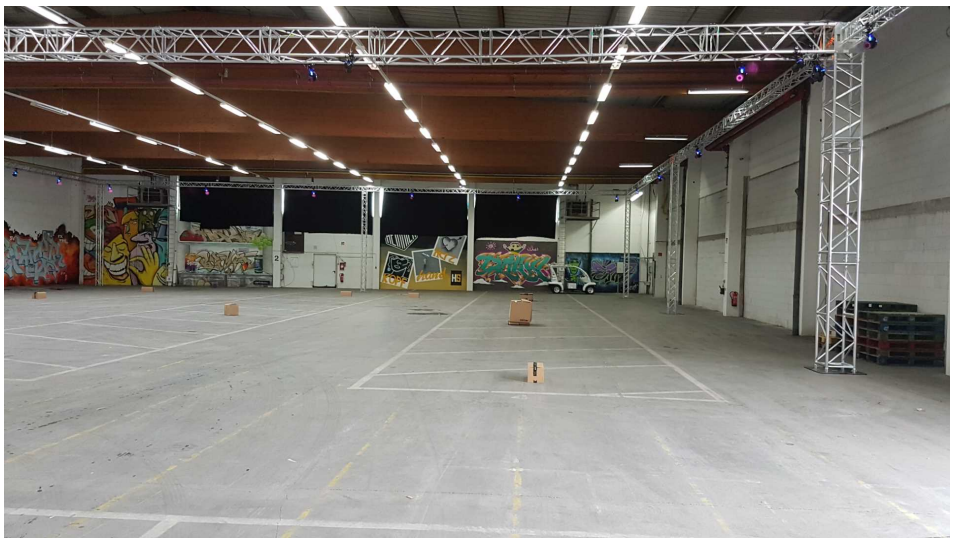

Figure 6.1: AIDA Hall test facility used for efficiency trials (image credit: Reutlingen University [**Reu24**]).

Documentation

All experiments were recorded through synchronized *rosbag* logs and video footage to facilitate data visualization and reproducibility. Post-processing and analysis were conducted in Python, using custom scripts for trajectory evaluation, energy estimation, and control performance comparison.

7 Experiments and Evaluation

We design experiments to validate thrust mapping, agility/controllability, aerodynamic disturbance characterization, and efficiency gains.

7.1 Thrust map identification

Throttle-to-thrust and RPM-to-thrust mapping; present identified curves and fitted models.

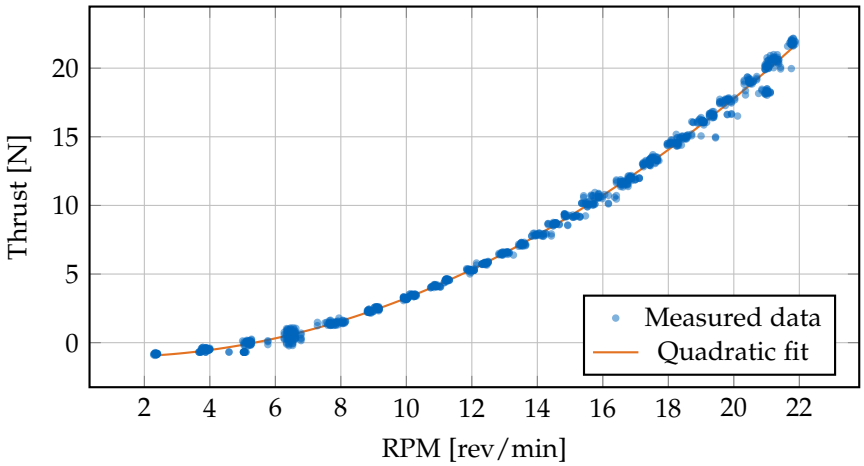

Figure 7.1: Thrust vs RPM with quadratic fit: $T = 0.0515 \cdot \mathrm{RPM}^2 - 0.0902 \cdot \mathrm{RPM} - 0.996$ (N). $R^2 = 0.997$.

7.2 Agility and tracking

- 3g circles in flight arena; metrics: RMS position/attitude tracking error, control effort.

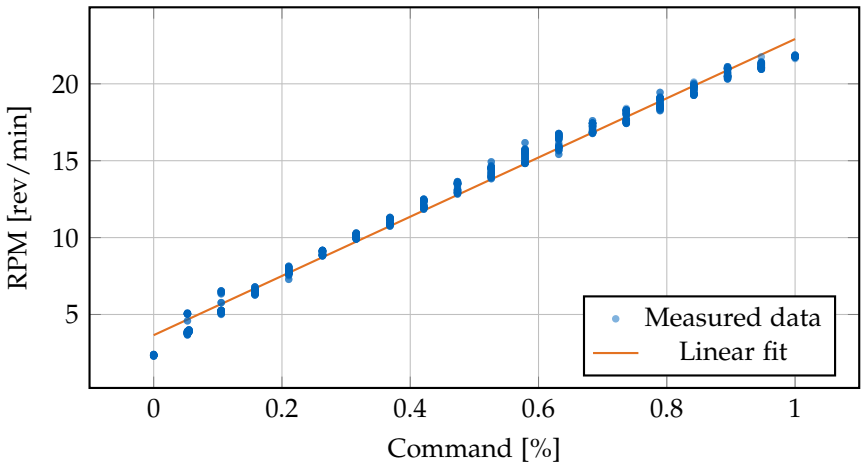

Figure 7.2: RPM vs Command with linear fit: $\text{RPM} = 19.26 \cdot \text{cmd} + 3.65$ (rev/min). $R^2 = 0.991$.

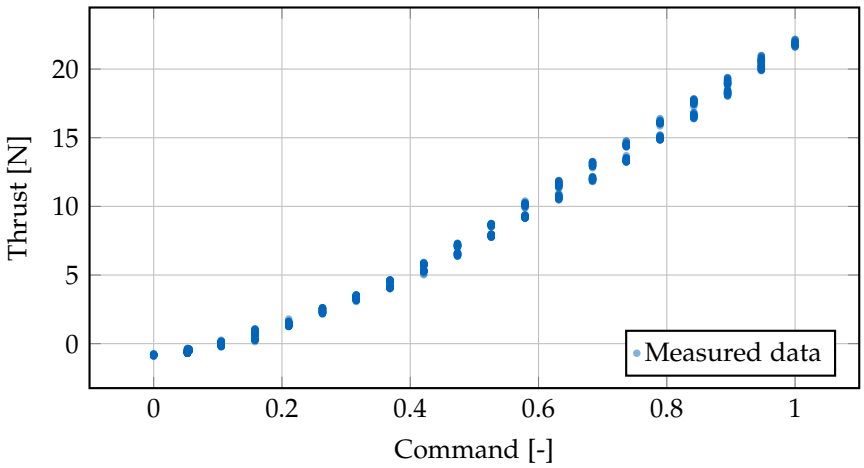

Figure 7.3: Thrust vs Command showing the direct relationship between motor command and thrust force.

7.3 Aerodynamic forces/moments quantification

- Identify equivalent k_D, k_L or $C_L(\alpha), C_D(\alpha)$ from maneuvering flight data; discuss sensitivity.

7.4 Efficiency assessment

- Compare theoretical quad thrust input vs. measured thrust input in AIDA hall flights; quantify energy savings due to passive lift.

7.5 Baseline comparison

- Compare against baseline quadrotor controller without INDI or without wings.

8 Conclusion

We summarize contributions: design of an aerodynamic surface-enhanced quadrotor, a robust INDI-based tracking controller, and experimental validation demonstrating accurate agile tracking and improved forward-flight efficiency. We outline future work, including refined aerodynamic modeling, coordinated-turn guidance integration, and extended outdoor testing.

Abbreviations

UAV Unmanned Aerial Vehicle
MAV Micro Air Vehicle
VTOL Vertical Take-Off and Landing
INDI Incremental Nonlinear Dynamic Inversion
EoM Equations of Motion
DoF Degrees of Freedom
CoG Center of Gravity
CoP Center of Pressure
IMU Inertial Measurement Unit
Vicon Vicon Motion Capture System
FC Flight Controller
ESC Electronic Speed Controller
RPM Revolutions per Minute

List of Figures

List of Tables